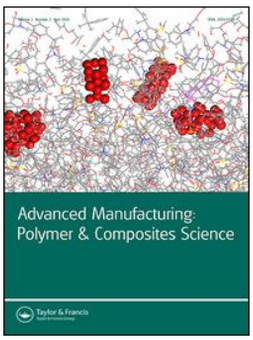

Taylor & Francis
Taylor & Francis Group

Advanced Manufacturing: Polymer & Composites Science

ISSN: 2055-0340 (Print) 2055-0359 (Online) Journal homepage: http://www.tandfonline.com/loi/yadm20

# Online monitoring of surface cracks and delaminations in carbon fiber/epoxy composites using silver nanoparticle based ink

**Till Augustin , Danny Grunert, Hauke H. Langner , Vico Haverkamp & Bodo Fiedler**

**To cite this article:** Till Augustin , Danny Grunert, Hauke H. Langner , Vico Haverkamp & Bodo Fiedler (2017) Online monitoring of surface cracks and delaminations in carbon fiber/epoxy composites using silver nanoparticle based ink, Advanced Manufacturing: Polymer & Composites Science, 3:3, 110-119, DOI: 10.1080/20550340.2017.1362508

**To link to this article:** http://dx.doi.org/10.1080/20550340.2017.1362508

AMPCS Advanced Manufacturing: Polymer & Composites Science

Original Research Paper

Check for updates

# Online monitoring of surface cracks and delaminations in carbon fiber/epoxy composites using silver nanoparticle based ink

**Till Augustin[1]*, Danny Grunert[1], Hauke H. Langner[2], Vico Haverkamp[2] and Bodo Fiedler[1]**

[1]Institute of Polymer and Composites, Hamburg University of Technology, Hamburg, Germany
[2]Institute of Automation Technology, Helmut Schmidt University, Hamburg, Germany



**Abstract** In this study, we present an online-monitoring approach using silver nanoparticle based ink on carbon fiber reinforced plastics (CFRP). After production of CFRP plates in a prepreg autoclave process and printing conductive paths on the material, we investigate the conductive paths of printed silver nanoparticle-based ink on CFRP by light microscopy. Mechanical tests with simultaneous electrical resistance measurements demonstrate the possibility to detect particular modes of failure with samples specifically designed to promote inter-fiber failures and delaminations under bending. Delaminations can be detected and localized inside the material by electrical through-thickness measurements and resistance measurements of the conductive paths allow for surface crack detection.

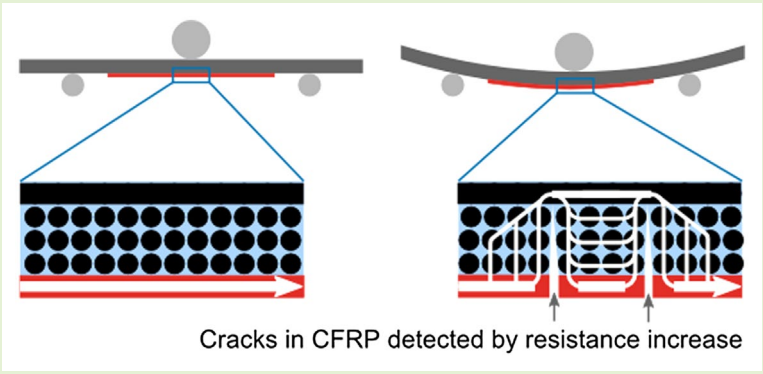


**Keywords:** Structural health monitoring, CFRP, ink-jet printing, conductive paths, inter-fiber failures, surface cracks, delaminations

**Cite this article** Till Augustin , Danny Grunert, Hauke H. Langner, Vico Haverkamp and Bodo Fiedler: *Adv. Manuf.: Polym. Compos. Sci.*, doi 10.1080/20550340.2017.1362508

## Introduction

Carbon fiber reinforced plastics (CFRP) are widely used in various industries such as aircraft, aerospace, automotive, and wind energy. To assure integrity and avoid catastrophic structural failures, periodic inspections are carried out, which can be time-consuming and costly especially for large structures due to expensive non-destructive testing (NDT) processes and downtime. Hence, a permanent monitoring of the integrity of the structure during operation, namely a structural health monitoring (SHM) system, is valuable in many cases. SHM offers a high potential to increase safety, reliability, and cost efficiency of fiber reinforced structures.

Several approaches for monitoring composite structures exist.[1–6] One promising SHM method for materials, which are not electrically insulating, is the electrical resistance measurement.[7] In CFRP, the carbon fibers are electrically conductive and the polymer matrix is non-conductive. The high electrical conductivity of carbon fibers allows for *in situ* strain monitoring and damage detection by electrical resistance measurements.[8–14]

To exploit the electrical conductivity of CFRP and use the material itself as a sensor in an SHM system a reliable contacting of the material is crucial to enable electrical resistance measurement during operation. Due to its excellent reproducibility and high potential for industrial automation, ink-jet printing is a promising technology to place conductive paths on the material and realize reliable contacts for electrical resistivity measurements.[15–19] Silver as ingredient in the ink for the conductive paths is favorable due to its high conductivity and in contrast to copper, it is a cost-efficient noble metal and a passivation is not necessary. Especially for nanoparticle-based inks, the corrosive properties of the used metal are not negligible due to the large surface area. A small

*Corresponding author, email till.augustin@tuhh.de



Received 16 February 2017; accepted 28 July 2017
DOI 10.1080/20550340.2017.1362508

particle size allows a strong reduction of the melting point,[20–22] and therefore a low sintering temperature is possible.[23] Low sintering temperatures for conductive paths allow to print electronics on temperature sensitive substrates like flexible electronics on foil.[17] Working with CFRP and silver inks a low sintering temperature is also essential to avoid damaging the material. Recently, researchers investigated the reduction of sintering time by using flash light sintering, which speeds up the manufacturing process and makes the approach even more attractive for industrial application.[24]

In the present work, we investigate a new approach to use ink-jet printed conductive paths on CFRP to detect and localize damages in the material. Silver nanoparticle-based ink is printed on CFRP specimens and sintered on the structure. Three-point bending tests with simultaneous electrical resistance measurements are carried out. X-ray and ultrasonic testing are used for a parallel detection and localization of the damages. The work aims to demonstrate the damage sensing potential of an electrode system, which is directly printed onto the CFRP surface with a focus on the detection and localization of inter-fiber failures and delaminations.

## Materials and specimen preparation

### CFRP specimens

The used carbon fiber reinforced prepregs consist of an epoxy matrix and carbon fibers (Hexply M21/34%/UD194/T800S by Hexcel) and have a fiber volume content of 57.77 ± 0.01% (measured on eight samples of the cured carbon fiber laminates according to DIN EN 2564). CFRP plates with the two different laminate layups, $[90_3/0_2]_S$ and $[90_3/+45/-45]_S$, were laminated from the prepregs and cured in an autoclave process at a temperature of 180 °C and a pressure of 7 bar for 120 min in a nitrogen atmosphere. The laminate layups were chosen to introduce inter-fiber failures on the bottom side of the specimens and delaminations in top of the lower three 90°-layers under bending conditions. Subsequently, specimens with dimensions of 100 mm × 15 mm × 1.9 mm (in accordance with DIN EN ISO 14125) were cut from the plates using a water-lubricated diamond saw. Additionally, for electrical characterization of the CFRP, a unidirectional (UD) laminate with the laminate layup $[0]_{10}$ was manufactured using the described autoclave process. From this plate specimens with dimensions of 15 mm × 15 mm were cut.

### Printed conductive paths

Functional silver-ink was printed on the CFRP surface to obtain conductive paths. No surface treatment was carried out prior to printing to keep the amount of manufacturing steps as low as possible. The surfaces were cleaned using isopropyl alcohol. Silver nanoparticles (31.0 wt.-%) with a D90 value (90% of the distribution lies below this value) of 60 nm were dispersed in the solvent butyl carbitol (68.5 wt.-%). The density of the ink is 1.48 g/ml and the viscosity measures 17.6 mPas at a shear rate of 1000 $s^{-1}$ at room temperature. For steric stabilization, 0.5 wt.-% ethyl cellulose was added which assures a stable suspension for about 3 h. Thus, during the printing process the composition of the ink is constant. The used single nozzle print head (by microdrop Technologies) has a nozzle diameter of 70 µm. A piezo actuator controls the emission of single drops. The voltage and the current pulse applied to the piezo actuator as well as the nozzle temperature can be varied to obtain an optimal drop. The control software and the moveable table where the substrate is placed to allow for printing images on the CFRP. This system forms a reliable and reproducible drop with the ink as described above. A sintering temperature of 170 °C was applied for 4 h to obtain conductive silver paths. Figure 1(a) shows the printing setup used. The printed conductive paths on the CFRP using this setup are shown in Figure 1(b) and (c) in different magnifications.

### Specimen preparation

To enable reliable contacting with the system for resistance measurements stranded copper wires were connected with the printed conductive paths using conductive silver paint (Acheson Silver DAG 1415M). Silver paint was also applied on the edges of the specimens that were used for electrical characterization. After finished preparation, the specimens were dried for 5 h at 40 °C in a vacuum oven and stored in a desiccator until testing to keep the specimen conditions constant.

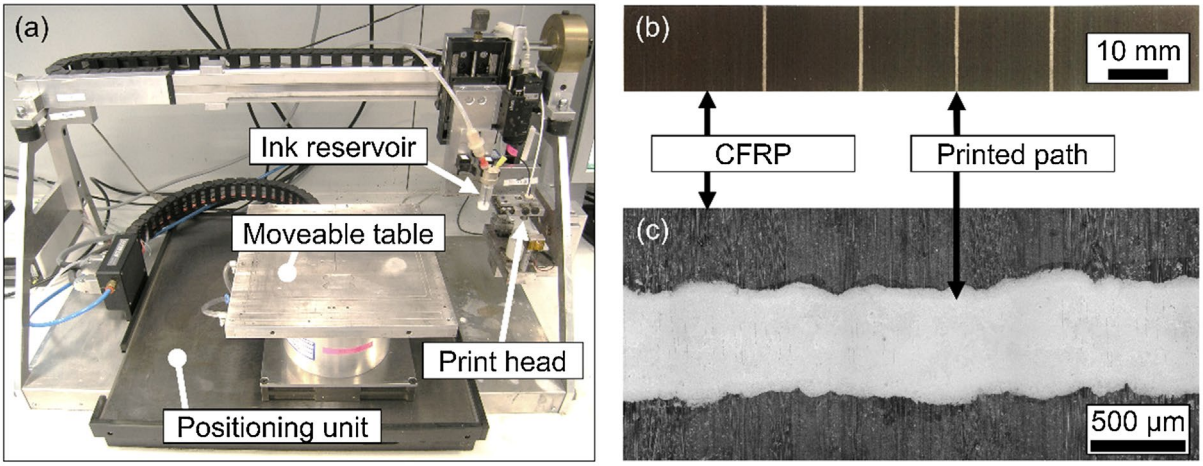


**Figure 1 (a) Ink-jet printing setup used, (b) Image of specimen with four printed conductive paths, and (c) Light microscopy observation of printed path prior mechanical testing**

# Experimental

## Electrical characterization

Four channel measurements were carried out to determine the conductivity of the UD CFRP specimens in three directions by using a digital multimeter (Keithley 2601A). Ten specimens were tested in the following three directions, respectively:

- In fiber direction (0°-direction)
- Perpendicular to fiber direction, in plane (90°-direction)
- Perpendicular to fiber direction, out of plane (thickness direction)

On each specimen, one continuous electrical measurement was carried out. From the resistance, $R$, the measuring length, $l$, and the cross section, $A$, the conductivity, $\sigma$, is calculated as follows:

$$\sigma = \frac{l}{R \cdot A}$$

Additionally, the conductivity of the printed silver nanoparticle-based paths was measured for comparison of the conductivity of path and CFRP substrate. Therefore, five specimens with insulating surfaces were investigated. On each specimen, one path with a length of 38.2 mm, a width of 0.67 mm, and a thickness of 7 µm was printed. A sintering of the conductive paths was conducted before electrical measurements. On each specimen, one continuous electrical measurement was carried out by connecting the digital multimeter (Keithley 2601A) with the ends of the conductive paths. From the number of specimens, $n$, the measured values, $x_i$, and the mean value, $\bar{x}$, the standard deviation, $s$, is calculated using the following equation:

$$s = \sqrt{\frac{1}{n-1}\sum_{i=1}^{n}(x_i - \bar{x})^2}$$

## Setup of mechanical and electrical tests

We conducted three-point bending tests using a universal testing machine (Zwick Z2.5 TH) to achieve high tensile loads in the lower 90°-layers and systematically introduce inter-fiber failures on the bottom side of the specimens and delaminations above the lower 90°-layers. The test speed was set to 2 mm/min to generate a sufficient time interval between the individual failures to detect the failures separately. Both, loading pin and supporting pins (further denoted as cylinders) of the three-point bending test setup consist of aluminum oxide ($Al_2O_3$) to ensure electric insulation of the specimens during testing. The distance between the lower cylinders was 55 mm and the diameters were 10 mm and 4 mm for the upper and lower cylinders, respectively.

Two different test series were conducted and are described in the following. In the first test setup conductive paths are printed parallel to the 100 mm long edges and the resistance is measured along these paths to investigate the change of resistance along the paths exposed to bending. In addition, tests with printed paths on both sides of the specimens are tested and the resistance is measured through the material during mechanical testing.

### *Electrical resistance measurements along printed paths*

The specimen geometry and the locations of the conductive paths are shown in Figure 2(a). Two paths are printed on the bottom side of the specimen. This design was chosen to be able to compare two measured signals from two paths lying next to each other. To measure the DC resistance over the length of the conductive paths the ends of the paths are connected with a digital multimeter (Keithley 2000). Figure 2(b) shows a schematic of the test setup.

### *Electrical resistance measurements through material*

To be able to measure the resistance through the material, specimens with printed paths on both sides are produced. The design of the conductive paths for measuring through the material is shown in Figure 3(a). The DC resistance is measured from the top electrode to each of the four electrodes on the bottom side of the specimen. Figure 3(b) shows the test setup and the connected electrodes for the four measured resistances.

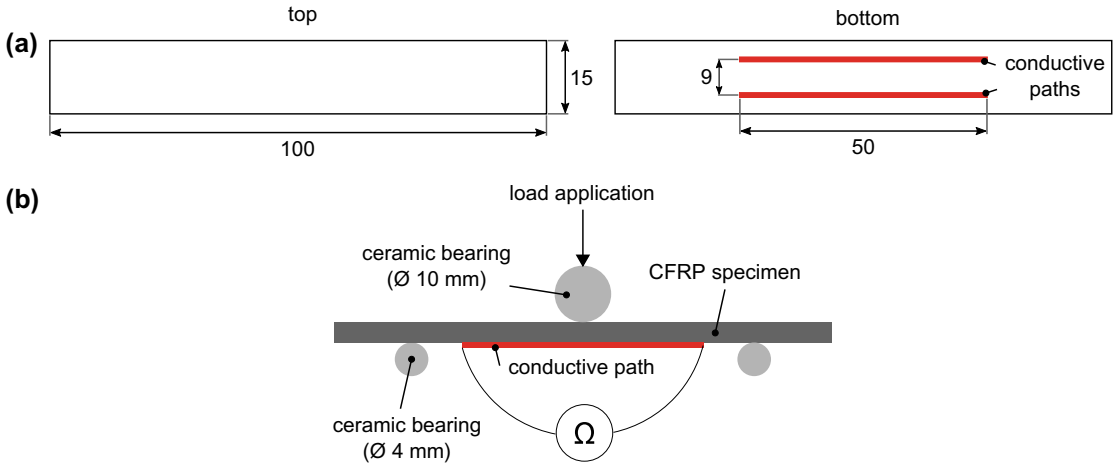


**Figure 2 (a) Specimen geometry, design of conductive paths for measuring resistance along printed paths, (b) Three-point bending test setup with electrical resistance measurement along printed paths**

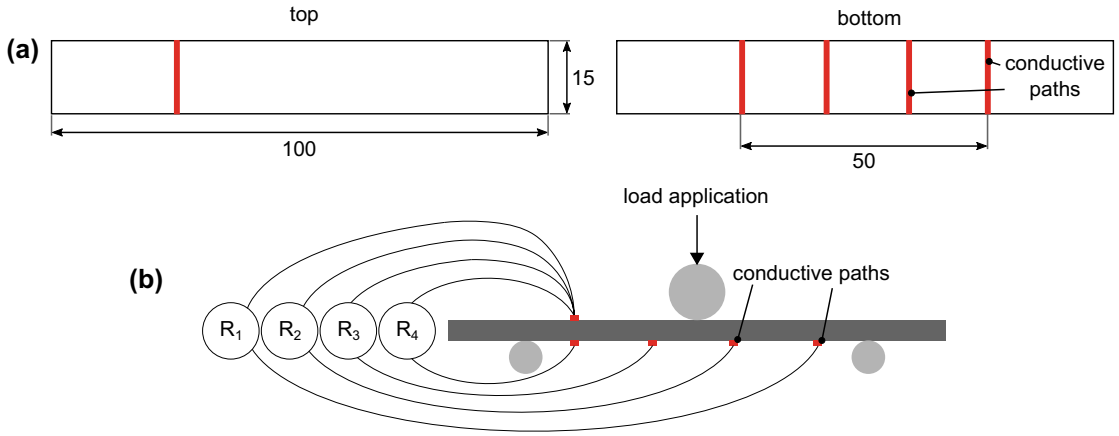


**Figure 3 (a) Specimen geometry, design of conductive paths for measuring resistance through material, (b) Three-point bending test setup with electrical resistance measurement through material**



## Nondestructive testing

### *X-ray testing*

Radiography was used for detection and localization of inter-fiber failures (Faxitron Model 43855a). The tube current was 3 mA at 20 keV and the exposure time of the D2 films was 5 min. For better visibility of cracks, a zinc iodide-based contrast medium, consisting of $ZnI_2$, $H_2O$, isopropyl alcohol, and Agfa Agepon, was applied on the specimen edges prior X-ray exposure. Development and fixing of the films was conducted using the manual developer Agfa Structurix G128 in conjunction with the fixer Agfa Structurix G328. Finally, the films were flushed in water for 10 min and dried in a drying chamber for 20 min.

### *Ultrasonic testing*

To evaluate locations and size of the delaminations at different load levels, ultrasonic measurements were carried out (USPC 3040 from Ingenieurbüro Dr Hillger). Pulse-echo method was used and demineralized water served as coupling medium. Selected specimens were tested at load levels with displacements from 0 mm up to 12.5 mm in displacement steps of 2.5 mm. Characterization of the delaminations were performed on the generated c-scans.

# Results

## Electrical conductivity

The conductivity values are shown in Table 1.

As expected, the highest conductivity is present in fiber direction and the conductivity perpendicular to the fiber direction in plane is higher than the conductivity perpendicular to the fiber direction in thickness direction (due to resin rich areas between the plies). The conductivity of a printed path is two orders of magnitude higher than the conductivity of the CFRP in fiber direction. This difference enables to measure changes of the current flow from the highly conductive paths to the lower conductive CFRP.

Electrical conductivity and in particular through-thickness electrical conductivity of CFRP varies extremely depending on fiber volume content and size of the inter-laminar polymer layers. Compared to the values presented here, much lower conductivities have been measured in some other studies.[25,26] In these studies, microscopy images show larger inter-laminar polymer layers than the light microcopy images of our investigated CFRP. However, there are also studies that report electrical conductivities in the same range[27] or even higher than the ones reported in our paper measured on comparable materials[9] even for interleaved systems.[27]

In the cross sectional view (see Figure 10) it can be seen that the inter-laminar polymer layers are relatively small and at some points touching fibers of adjacent layers can be observed. In combination with the high fiber volume content, this leads to a relatively high through-thickness conductivity.

A comparison of the through-thickness conductivity of UD and quasi isotropic laminates supports this observation. We measured through-thickness conductivities of quasi isotropic laminates (laminate layup: $[45/0/-45/90]_s$) made from the same prepregs using the same amount of specimens and found an electrical conductivity in through-thickness direction of 3.3 ± 0.3 S/m which is twice as high as the conductivity measured on the UD specimens. The higher conductivity of the quasi isotropic laminates is present due to more connection points of touching fibers of adjacent layers compared to UD laminates. Other researchers have also observed this trend before by comparing UD and multi-directional laminates.[28]

**Table 1 Electrical conductivities of unidirectional specimens, $[0]_{10}$, in three directions and printed silver nanoparticle-based sintered path on insulating substrate in S/m.**

| | Fiber direction | Transverse direction, in plane | Through-thickness direction | Silver nanoparticle ink, sintered |
|---|---|---|---|---|
| Mean value in S/m | $3.7 \cdot 10^3$ | $1.5 \cdot 10^1$ | $1.4 \cdot 10^0$ | $4.9 \cdot 10^5$ |
| Standard deviation in S/m | $0.4 \cdot 10^3$ | $0.4 \cdot 10^1$ | $0.4 \cdot 10^0$ | $0.9 \cdot 10^5$ |

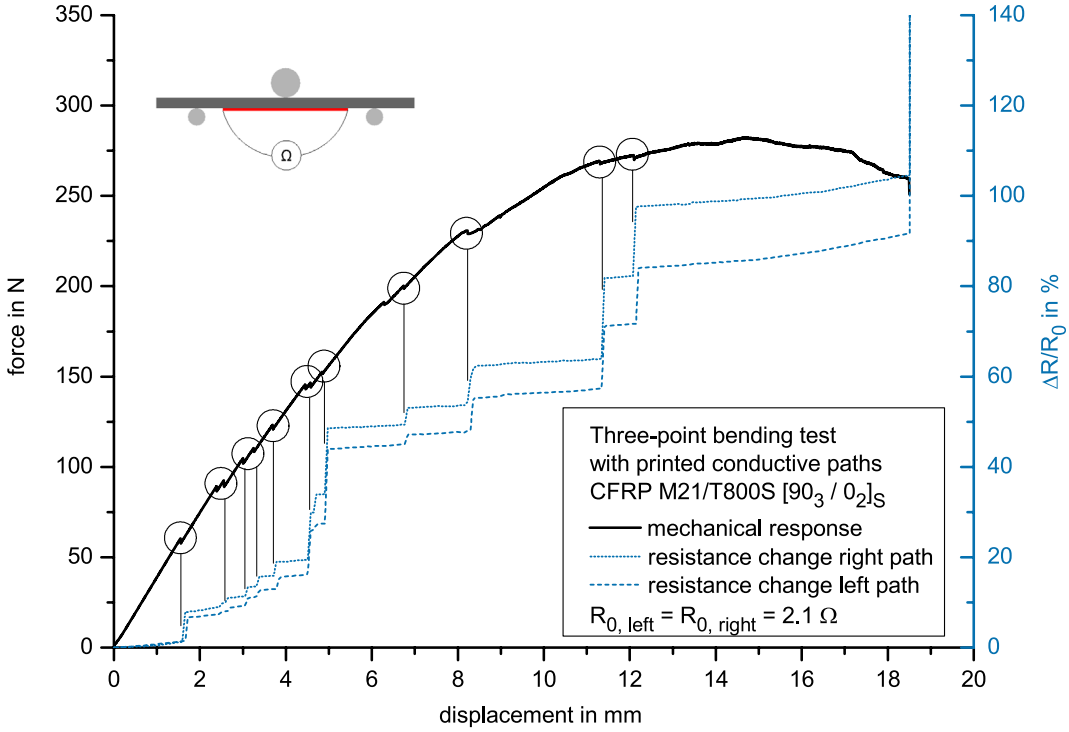


**Figure 4 Force and resistance change of conductive paths versus displacement, $[90_3/0_2]_S$ laminate**

## Electrical resistance measurements along printed paths for surface crack detection

Figure 4 shows typical results of the mechanical and electrical measurements for a specimen with a layup of $[90_3/0_2]_S$. The resistance without loading ($R_0$) is 2.1 Ω for both conductive paths, and the resistance change ($\Delta R$) is specified as the difference of the measured resistance without ($R_0$) and during loading ($R$).

The force increases to a maximum at a displacement of 14.8 mm and fracture of the specimen occurs at 18.7 mm. In addition to the mechanical response, the change of electrical resistance is shown for the two conductive paths, measured from one end to the other of the same path, respectively. Both, the force-displacement curve and the resistance change-displacement curves contain several discontinuities indicated by circles in the diagram. The discontinuities correlate perfectly with the steps in the resistance change.

The discontinuities in the measured force are present due to damages in the material. Since the dominating failure modes in cross-ply laminates subjected to bending and the failures observed in the tested specimens are inter-fiber failure and delamination, these two failure modes lead to the discontinuities of the measured force and resistance signals. All failures detected by the measured force exceeding a certain amount of energy release can be detected by resistance changes. X-ray images show that all discontinuities in the mechanical response correlate to inter-fiber failures and the developing delaminations show no distinct discontinuities. The resistance increase at the end of the test (up to unmeasurable values) indicates the final fracture of the specimen cutting the specimen completely and therefore all possible conductive paths for current flow. Hence, all failures exceeding a certain size and therefore being relevant for the integrity of the specimen as well as the final fracture can be detected reliably.

Light microscopy observations of the damaged printed paths show that inter-fiber failures at the surface cause interruptions as well as flaking of the paths in proximity to the cracks (see Figure 5). Hence, when inter-fiber failures occur the resistance increases due to the interruption of the paths in the region of the cracks at the surface. The current flow in case of inter-fiber failures flows through the CFRP, which has a higher resistance compared to the silver-based printed path resulting in a resistance increase. The current flow is schematically shown in Figure 6. This method enables to detect inter-fiber failures reliably on the surface. It can be used to monitor surfaces where surface cracks are crucial. Damages of the paths occurred only due to events of inter-fiber failures and no debonding of the CFRP-silver interface could be observed. Therefore, the quality of the interface is sufficient for the considered application even without additional surface treatment.

The 0°-fibers in the cross-ply laminate have a significant influence on the mechanical as well as on the electrical behavior. Therefore, a substitution of the 0°-layers with ±45°-layers was conducted and the results are shown in Figure 7. Due to the different layup, the maximum force and the Young's modulus are reduced and less inter-fiber failures occur. The resistance change is similar compared with the resistance change of the cross-ply laminate, shown in Figure 4.

It can be said that with the substituted middle layers the surface cracks can be detected reliably as well. Therefore, a detection of all inter-fiber failures is possible for both, 0°-layers and ±45°-layers as middle layers of the laminate.

For both laminates, the increase of the resistance varies significantly for differently located inter-fiber failures. Therefore, specimens are tested and unloaded at every inter-fiber failure event and X-ray images are made to correlate the location of the damage with the resistance increase that the damage

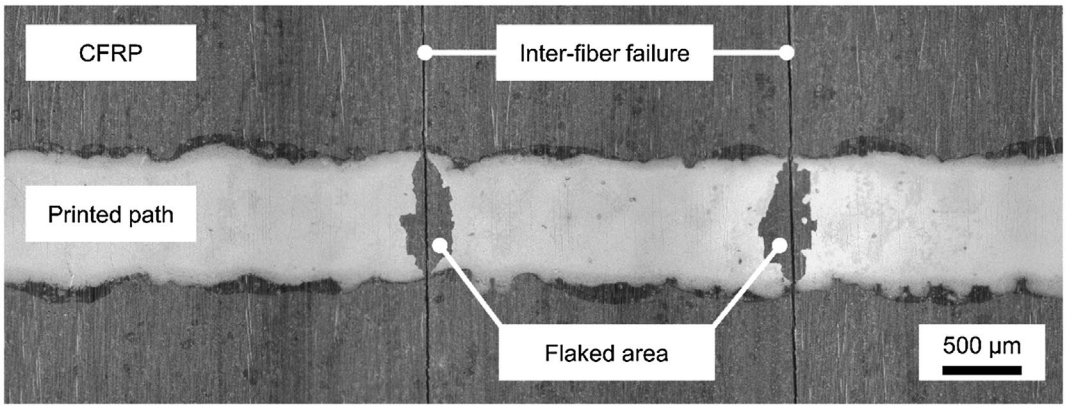


**Figure 5 Light microscopy observation of printed path after testing**

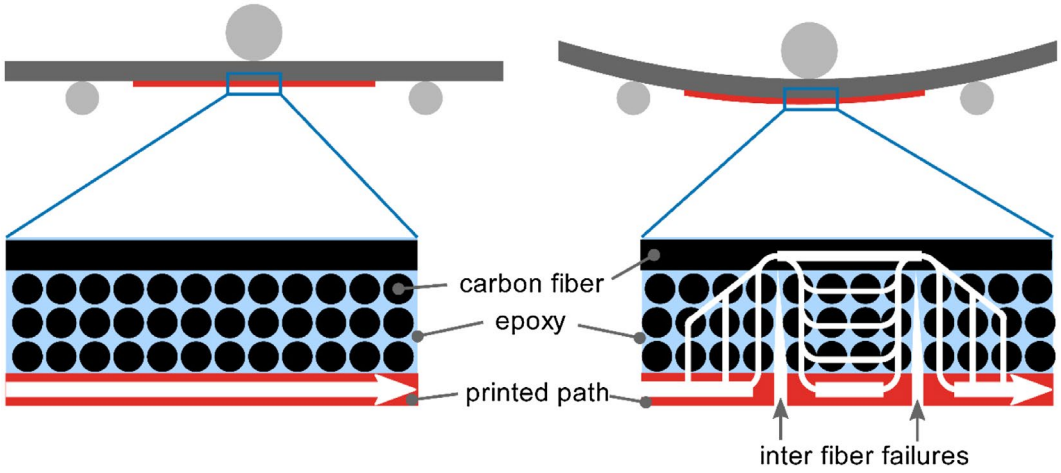


**Figure 6 Schematic of current flow (white arrows); left: through undamaged printed path; right: through damaged printed path and composite material in case of inter-fiber failures**

causes (see Figure 8). At the first damage event, two inter-fiber failures occur and the resistance increases 4.1%. For the third inter-fiber failure the resistance increases clearly as well. The next two inter-fiber failures, which are present in between two existing inter-fiber failures (test steps 3 and 4) show only small increase in resistance. The last inter-fiber failure does not lie in between two inter-fiber failures and leads to a significant increase of the resistance again.

Inter-fiber failures that lie in between two other inter-fiber failures lead to a smaller resistance increase compared to the inter-fiber failures that do not lie in between two other inter-fiber failures. Failures in between two other failures do not change the current flow as much as failures outside of other failures, since the path of least resistance is not changed in the case of a new crack in between two other cracks.

Hence, a reliable detection of inter-fiber failures with the presented approach is possible. However, a localization of the damage is only possible when multiple paths with different electrode locations are used.

## Electrical measurement through material for delamination detection

Mechanical and electrical measurements for a typical behaving specimen are plotted in Figure 9. The mechanical response is qualitatively the same as in Figure 4. The resistance changes are different for the four measured channels. For channel 1 (from top electrode to low electrode 1) and channel 4 (from top electrode to low electrode 4) the relative resistance change is in the range of ±2.5% until final fracture, where the resistances suddenly increase to infinity. The resistance change of channels 2 and 3 (from top electrode to lower middle electrodes) increases significantly with increasing displacement up to 26% and 17.5% before final failure, respectively.

The non-significant resistance changes of channel 1 and 4 (to electrodes left and right of the specimens) indicate that the current flow is not changed significantly in these areas of the specimen. It is assumed that close to these electrodes no delaminations and inter-fiber failures that interrupt the current flow are present. For channel 2 and 3 the resistance increase indicates that damages occur inside of the material close to the most stressed areas in the center of the specimen. This can be proven by light microscopy observations of a tested specimen shown in Figure 10. Above electrodes 2 and 3 (center electrodes), inter-fiber failures in the three lower 90°-layers and delaminations in between the 0°- and 90°-layer are found. Above the outer electrodes (1 and 4) only inter-fiber failures are detected by light microscopy.

The comparison of the regions close to the outer electrodes and close to the inner electrodes shows that the only

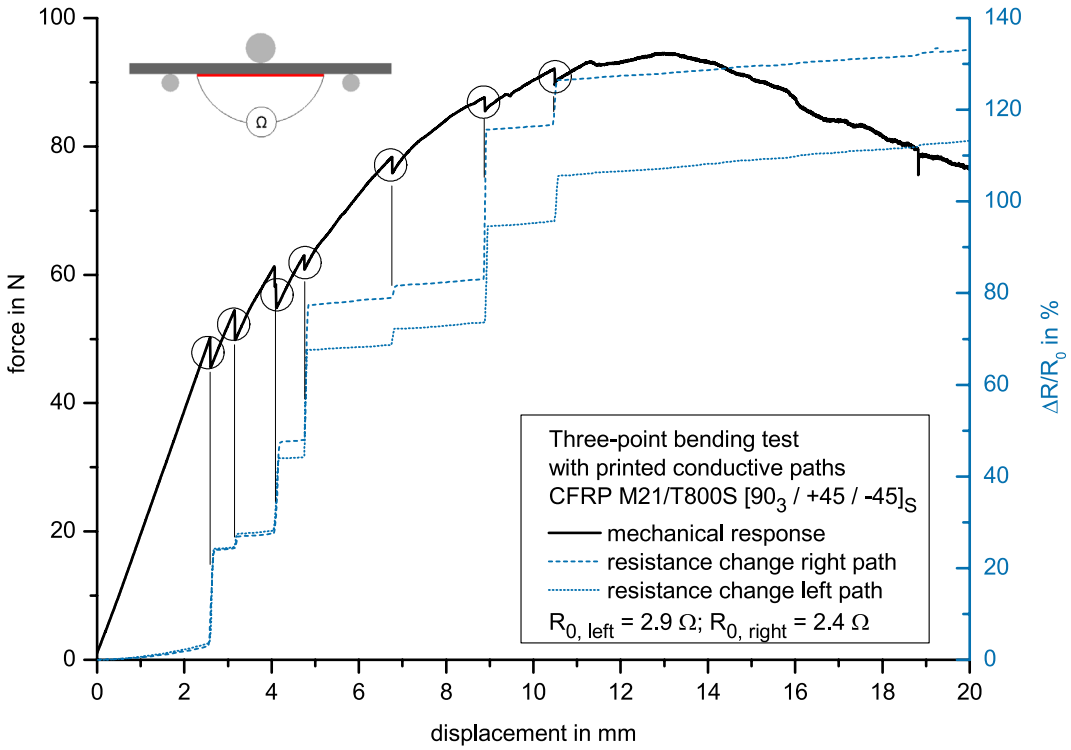


**Figure 7 Force and resistance change of conductive paths versus displacement, $[90_3/+45/-45]_s$ laminate**

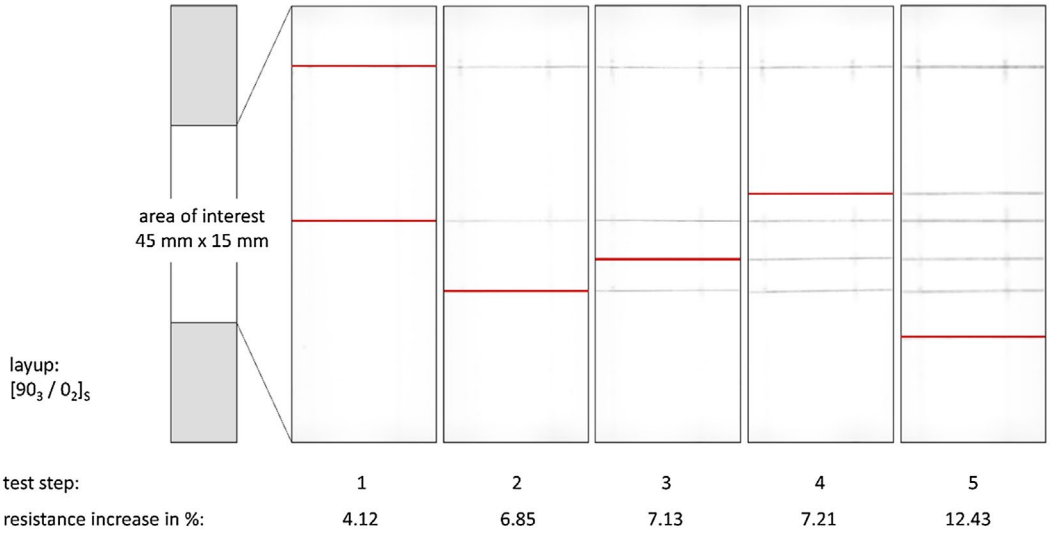


**Figure 8 X-ray images of loaded specimen showing the development of inter-fiber failures and the according measured resistance increase**

difference is the presence of delaminations in the higher loaded (center) area. Inter-fiber failures in the 90°-layers are present in all areas. Since the resistance change increases only for measurements with electrodes close to the most loaded areas where delaminations occur, delaminations can be detected by a significantly higher resistance change compared to areas where only inter-fiber failures occur, which are not detected by the through-thickness measurements.

C-scans from ultrasonic testing show the development of delaminations (see Figure 11). No delaminations are present at 2.5 mm displacement. First delaminations are detected at 5.0 mm displacement. Between these two loading steps the resistance, measured to the middle electrodes, increases significantly. Hence, a detection of the first delaminations by resistance increase is possible. With increasing displacement both, the delaminations and the resistance for the electrodes that are close to delaminations increase. Furthermore, we found that the delaminations appear in a depth of about 1.3 mm, which is the location of the lower 0°/90°-interface, since the cured ply thickness is 0.19 mm, resulting in a depth

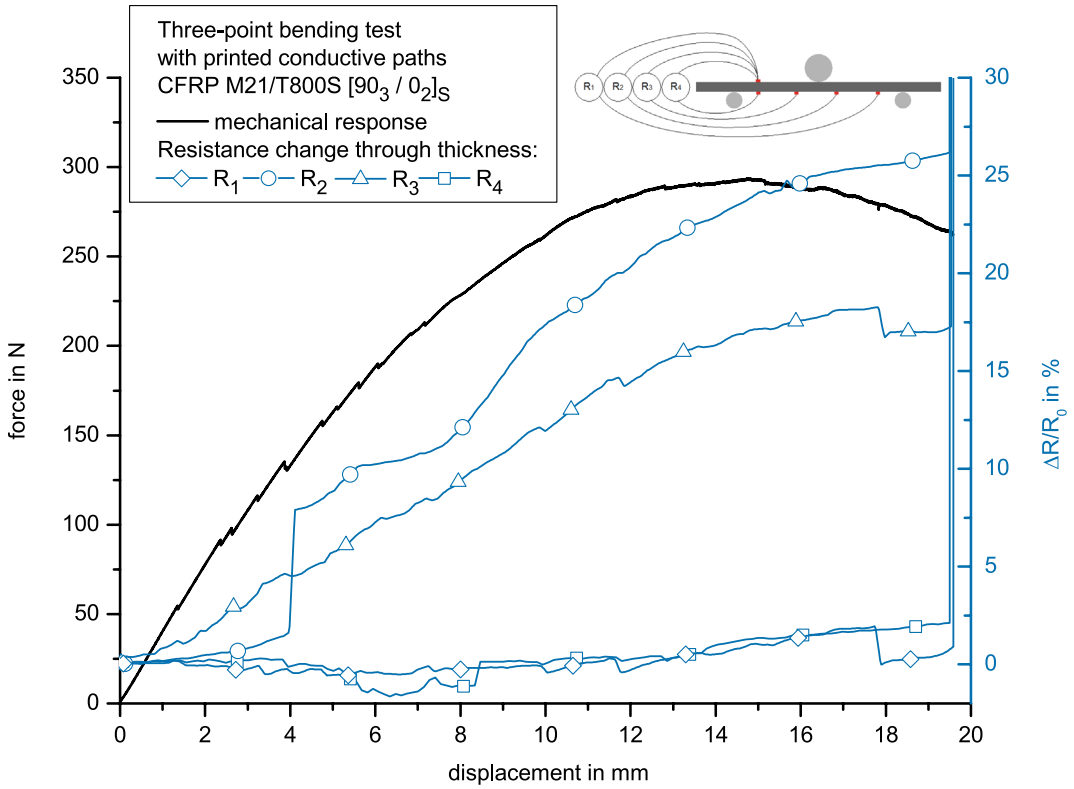


**Figure 9** Force and resistance change of the four measured channels versus displacement

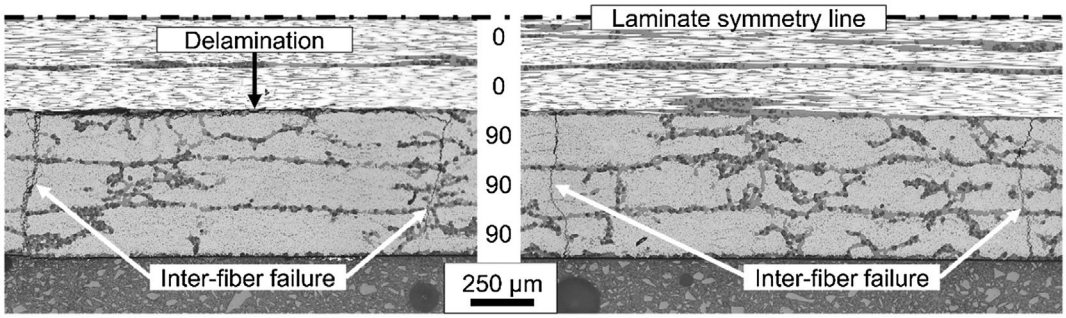


**Figure 10** Light microscopy observation of polished sections after testing. Left: Region above electrodes 2 and 3 (middle electrodes), inter-fiber failures and delaminations. Right: Region above electrodes 1 and 4 (outer electrodes), only inter-fiber failures

of the interface of 1.3 mm. This delamination area corresponds to the location of the delaminations found in light microscopy observation (see Figure 10).

Hence, detection as well as a localization of delaminations is possible with the used path design and through-thickness resistance measurement, since delaminations lead to a resistance increase at delamination areas in thickness direction.

## Application and future studies

Depending on the application, it might be necessary to consider the environmental conditions because temperature and humidity have an influence on the electrical resistance of CFRP. To determine an accurate damage location over a changing temperature/humidity profile it is necessary to know the influence of these parameters on the resistance of the considered structure. In practice, this can be achieved for instance by measuring the resistance of the monitored structure over a reasonable temperature range.

The path designs chosen within this study consist exclusively of linear geometries. These simple geometries were chosen to investigate paths parallel and perpendicular to the fiber direction to be able to differentiate between these two types of conductive paths. However, with the used inkjet technology, more complex conductive path geometries such as branched networks are printable as well. Furthermore, printing onto curved surfaces is possible. Depending on the curvature, a print head mounted on a robotic arm could be useful. It has to be noted that for thicker parts, a sufficient through-thickness conductivity needs to be guaranteed. In case of the presence of structural features (e.g. stringers), a

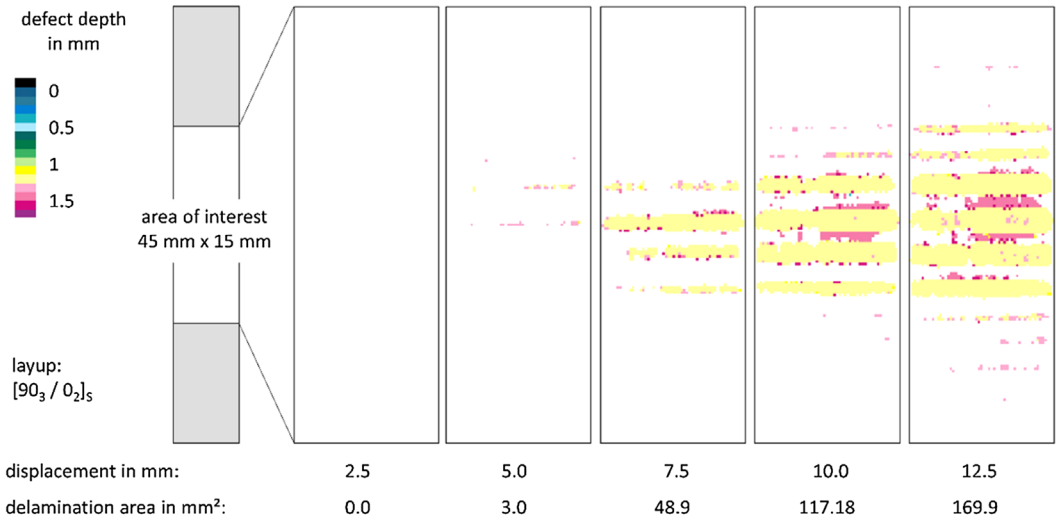


**Figure 11 Ultrasonic c-scans with depth information for different displacement steps in three-point bending test showing delaminations**

division into different systems monitoring parts and joints independently might be necessary. In addition, the sensitivity of the polymer matrix influences the measured resistances because damages monitored here are matrix dominated (e.g. toughening agents influence the crack propagation of matrix cracks). Using carbon nanoparticles in the polymer matrix an increase of the through-thickness electrical conductivity needs to be considered.

When applied in structures with integrated lightning protection the conductive paths need to be arranged in a way that they do not significantly change the current flow caused by lightning. However, existing metal foils or meshes used for lightning protection can act as two-dimensional electrodes and be integrated into the online-monitoring system for through-thickness electrical resistance measurements.

For future studies, the two following issues are of interest:

First, the presented ink-jet technology can be used to apply a conductive path network for monitoring of secondary bonded components and adhesives. To transfer the presented online-monitoring approach to a secondary bonding, the adhesive needs to be electrically conductive. Monitoring of adhesives is of particular interest, since it offers potential to increase the reliability of adhesively bonded joints.

Second, in addition to printing onto the cured CFRP, printing directly onto the prepregs is a promising approach. The printing process could be integrated into or done parallel to automated tape laying of prepregs and therefore minimize costs for printing. To obtain good conductive paths without gaps it is necessary to vacuum-bag consolidate the prepregs. This causes a surface that is smooth enough for the ink-jet printing process. A challenge for this approach is the low viscosity of the resin during an autoclave process. Possibly, the low viscosity of the resin can lead to insufficient quality of the printed paths after curing. This should be part of further investigations.

## Conclusion

Ink-jet printed silver nanoparticle ink on CFRP allows for *in situ* monitoring and detection of both, surface cracks and delaminations inside of the CFRP. If inter-fiber failures occur on the surface, the electrical resistance measured along single printed paths increases due to interruptions of the printed paths, which have a significantly lower resistance than CFRP. Failures inside of the material can be detected by measuring the electrical resistance through the CFRP. With through-thickness measurements delaminations can be detected by an increase of the electrical resistance. If multiple electrodes are printed on the material surface and several measurements are conducted synchronously, a localization of the defects is possible. Hence, in case of tailored designs of printed paths additionally to the detection also a localization of inter-fiber failures and delaminations in CFRP is possible.

## Disclosure statement

The authors reported no potential conflict of interest.

## Funding

This work was financially supported by the Landesforschungsförderung Hamburg (project 'Health-Monitoring von Faserverbundstrukturen mit Hilfe von Sensorarrays') [grant number LFF-FV 05]; the German Research Foundation (DFG) and the Hamburg University of Technology (TUHH) in the funding program 'Open Access Publishing'.

## ORCID

*Augustin Till* http://orcid.org/0000-0002-1953-1624
*Langner Hauke H.* http://orcid.org/0000-0003-4443-3919
*Fiedler Bodo* http://orcid.org/0000-0002-2734-1353

## References

1. K. Diamanti and C. Soutis: 'Structural health monitoring techniques for aircraft composite structures,' *Prog. Aerospace Sci.*, 2010, **46**, (8), 342–352.
2. M. Majumder, T. K. Gangopadhyay, A. K. Chakraborty, K. Dasgupta and D. K. Bhattacharya: 'Fibre Bragg gratings in structural health monitoring – present status and applications,' *Sens. Actuators, A*, 2008, **147**, (1), 150–164.

3. S. S. Kessler, S. M. Spearing and C. Soutis: 'Damage detection in composite materials using Lamb wave methods,' *Smart Mater. Struct.*, 2002, **11**, (2), 269–278.
4. J. Cai, L. Qiu, S. Yuan, L. Shi, P. Liu and D. Liang: 'Structural health monitoring for composite materials' in 'Heterogeneous composites on the basis of microbial cells and nanostructured carbonized sorbents', (ed. Zulkhair Mansurov *et al.*), 37–60; 2012, Rijeka, INTECH Open Access Publisher.
5. W. J. Staszewski, C. Boller and G. R. Tomlinson: 'Health monitoring of aerospace structures', 2003, Chichester, John Wiley & Sons Ltd.
6. I. Kang, M. J. Schulz, J. H. Kim, V. Shanov and D. Shi: 'A carbon nanotube strain sensor for structural health monitoring,' *Smart Mater. Struct.*, 2006, **15**, (3), 737–748.
7. D. D. L. Chung: 'Structural health monitoring by electrical resistance measurement,' *Smart Mater. Struct.*, 2001, **10**, (4), 624–636.
8. K. Schulte and C. Baron: 'Load and failure analyses of CFRP laminates by means of electrical resistivity measurements,' *Composites Sci. Technol.*, 1989, **36**, (1), 63–76.
9. J. Abry: '*In situ* detection of damage in CFRP laminates by electrical resistance measurements,' *Compos. Sci. Technol.*, 1999, **59**, (6), 925–935.
10. J. Wen, Z. Xia and F. Choy: 'Damage detection of carbon fiber reinforced polymer composites via electrical resistance measurement,' *Compos. Part B: Eng.*, 2011, **42**, (1), 77–86.
11. A. Kaddour, F. Al-Salehi, S. Al-Hassani and M. Hinton: 'Electrical resistance measurement technique for detecting failure in CFRP materials at high strain rates,' *Compos. Sci. Technol.*, 1994, **51**, (3), 377–385.
12. R. Schueler, S. P. Joshi and K. Schulte: 'Damage detection in CFRP by electrical conductivity mapping,' *Compos. Sci. Technol.*, 2001, **61**, (6), 921–930.
13. M. Kupke, K. Schulte and R. Schüler: 'Non-destructive testing of FRP by dc and ac electrical methods,' *Compos. Sci. Technol.*, 2001, **61**, (6), 837–847.
14. K. Takahashi and H. T. Hahn: 'Towards practical application of electrical resistance change measurement for damage monitoring using an addressable conducting network,' *Struct. Health Monit.*, 2012, **11**, (3), 367–377.
15. H.-H. Lee, K.-S. Chou and K.-C. Huang: 'Inkjet printing of nanosized silver colloids,' *Nanotechnology*, 2005, **16**, (10), 2436–2441.
16. P. J. Smith, D.-Y. Shin, J. E. Stringer, B. Derby and N. Reis: 'Direct ink-jet printing and low temperature conversion of conductive silver patterns,' *J. Mater. Sci.*, 2006, **41**, (13), 4153–4158.
17. J. Perelaer, C. E. Hendriks, A. W. M. de Laat and U. S. Schubert: 'One-step inkjet printing of conductive silver tracks on polymer substrates,' *Nanotechnology*, 2009, **20**, (16), 165303.
18. H. S. Kim, J. S. Kang, J. S. Park, H. T. Hahn, H. C. Jung and J. W. Joung: 'Inkjet printed electronics for multifunctional composite structure,' *Compos. Sci. Technol.*, 2009, **69**, (7–8), 1256–1264.
19. K. Rajan, I. Roppolo, A. Chiappone, S. Bocchini, D. Perrone and A. Chiolerio: 'Silver nanoparticle ink technology: state of the art,' *Nanotechnol. Sci. Appl.*, 2016, **9**, 1–13.
20. P. Buffat and J.-P. Borel: 'Size effect on the melting temperature of gold particles,' *Phys. Rev. A*, 1976, **13**, (6), 2287–2298.
21. G. L. Allen, R. A. Bayles, W. W. Gile and W. A. Jesser: 'Small particle melting of pure metals,' *Thin Solid Films*, 1986, **144**, (2), 297–308.
22. C. Y. Lai, C. F. Cheong, J. S. Mandeep, H. B. Abdullah, N. Amin and K. W. Lai: 'Synthesis and characterization of silver nanoparticles and silver inks: review on the past and recent technology roadmaps,' *J. Materi. Eng. Perform.*, 2014, **23**, (10), 3541–3550.
23. A. L. Dearden, P. J. Smith, D.-Y. Shin, N. Reis, B. Derby and P. O'Brien: 'A low curing temperature silver ink for use in ink-jet printing and subsequent production of conductive tracks,' *Macromol. Rapid Commun.*, 2005, **26**, (4), 315–318.
24. K. Takahashi, K. Namiki, T. Fujimura, E.-B. Jeon and H.-S. Kim: 'Instant electrode fabrication on carbon-fiber-reinforced plastic structures using metal nano-ink via flash light sintering for smart sensing,' *Compos. Part B: Eng.*, 2015, **76**, 167–173.
25. Y. Hirano, T. Yamane and A. Todoroki: 'Through-thickness electric conductivity of toughened carbon-fibre-reinforced polymer laminates with resin-rich layers,' *Compos. Sci. Technol.*, 2016, **122**, 67–72.
26. A. Lonjon, P. Demont, E. Dantras and C. Lacabanne: 'Electrical conductivity improvement of aeronautical carbon fiber reinforced polyepoxy composites by insertion of carbon nanotubes,' *J. Non-Cryst Solids*, 2012, **358**, (15), 1859–1862.
27. S. Wang, R. Downes, C. Young, D. Haldane, A. Hao, R. Liang, B. Wang, C. Zhang and R. Maskell: 'Carbon fiber/carbon nanotube buckypaper interply hybrid composites: manufacturing process and tensile properties,' *Adv. Eng. Mater.*, 2015, **17**, (10), 1442–1453.
28. S. Wang and D. D. L. Chung: 'Electrical behavior of carbon fiber polymer-matrix composites in the through-thickness direction,' *J. Mater. Sci.*, 2000, **35**, (1), 91–100.